

Nuclear and magnetic structure of an epitaxial $\text{La}_{0.67}\text{Sr}_{0.33}\text{MnO}_3$ film using diffraction methods

H. Himanshu,^{1,2} E. Rebolini,^{3,*} K. Beauvois,⁴ S. Grenier,⁵ B. Mercey,⁶
B. Domenges,^{6,†} B. Ouladdiaf,³ M. B. Lepetit,^{1,5} and C. Simon²

¹*Institute Laue-Langevin, 71 avenue des Martyrs, 38000 Grenoble, France*

²*Laboratoire National des Champs Magnétiques Intenses (LNCMI-CNRS, Université Grenoble Alpes), 25 avenue des Martyrs, 38000 Grenoble, France*

³*Institute Laue-Langevin, 71 avenue des Martyrs, 38000 Grenoble, France*

⁴*Commissariat à l'Énergie Atomique (CEA), IRIG, MEM, MDN, Univ. Grenoble Alpes, 38000 Grenoble, France*

⁵*Institut Néel (CNRS), 25 avenue des Martyrs, 38000 Grenoble, France*

⁶*CRISMAT, ENSICAEN-CNRS UMR6508, 6 bd. Maréchal Juin, 14050 Caen, France*

(Dated: December 5, 2023)

We use a combination of transmission electron microscopy, X-Ray and neutron diffraction, SQUID magnetometry and symmetry analysis to determine the nuclear and magnetic structure of an epitaxial LSMO film, deposited on a Si substrate. The film undergoes a magnetic ordering transition at 260 K. At 300 K, in the paramagnetic phase, the manganite film has a $I4/m$ space group. In the magnetic phase, SQUID and neutron diffraction results lead us to assign a ferromagnetic spin-order to the film, associated to magnetic moments with a slightly out-of-plane component, namely $(3.5, 0, 0.3) \mu_B$. Symmetry analysis further shows that only the $P\bar{1}'$ group is compatible with such a magnetic ordering.

I. INTRODUCTION

Doped perovskite manganites of general formula $\text{RE}_{1-x}\text{AE}_x\text{MnO}_3$ (RE: Rare Earth, AE: Alkaline Earth) have attracted considerable interest owing to their rich phase diagrams [1–6]. The complex interplay of charge, lattice, spin and orbital degrees of freedom is particularly interesting in $\text{La}_{1-x}\text{Sr}_x\text{MnO}_3$ bulk compounds. At a doping level of $x = 0.33$ ($\text{La}_{0.67}\text{Sr}_{0.33}\text{MnO}_3$ - LSMO), these compounds are found to be half-metallic ferromagnets below 370 K, and insulating in the paramagnetic phase [7, 8]. This behavior can be explained using the double-exchange mechanism and the Jahn-Teller effect in the Mn^{3+} ions [9]. In addition, colossal magneto-resistive effects were established in these materials [10, 11]. These properties make LSMO a promising candidate for many spin-based and electronic devices. The suitability of thin films for such applications causes a surge of interest in miniaturization of these bulk systems.

In epitaxial thin films, the substrate imposes a strain on the system, adding an additional degree of freedom. Due to the double-exchange mechanism, this substrate-strain greatly modifies the film properties compared to the bulk. As a consequence, the electronic and magnetic properties of LSMO films can be largely manipulated by the substrate choice, the film thickness and growth conditions [12–17]. Although the dramatic changes in LSMO film properties have been well-studied, there is no exact crystallographic knowledge, despite the high focus of research on correlation between LSMO films physical properties and structural modifications with respect to bulk [18–23]. The huge potential of these films for technological applications thus demands a complete nuclear and magnetic structure determination.

In this letter, we present our results obtained on a LSMO film of thickness 40.9 nm grown on a Si substrate. Such films on Si substrate are a usual request in semiconductor industry. A buffer layer of SrTiO_3 (STO) was deposited in-between the substrate and the film, in order to promote a better growth of LSMO. We studied the film magnetization along different directions, as a function of temperature and applied field, using an MPMS XL Quantum Design SQUID magnetometer at Institut Néel. Furthermore, single crystal X-ray diffraction (XRD at SmartLab, CEA-CNRS, Grenoble) and neutron diffraction (ND at D10 and D10+ at ILL, Grenoble) experiments were performed on the epitaxial film. We provide the detailed analysis for the determination of the atomic structure and magnetic configuration of the film.

II. EXPERIMENT

A. Thin film synthesis

The LSMO film was deposited using pulsed-laser deposition (PLD) on a Si substrate with in-situ Reflection High Energy Electron diffraction at CRISMAT laboratory, Caen. First, 20 unit cells of a STO buffer layer were deposited using PLD (at 650° C, in 1.6×10^{-5} mbar pressure) on top of the already Molecular Beam Epitaxy-deposited STO. Then, the deposition of 400 Å of $\text{La}_{0.67}\text{Sr}_{0.33}\text{MnO}_3$ (104 unit cells) was carried out, at 650° C in a pressure of 4.2×10^{-4} mbar, and an atmosphere of 0.1%-volume ozone in oxygen. The deposited film was cooled in an atmosphere of 5.9×10^{-3} mbar pressure with a mixture of ozone (7% volume) and oxygen. The cooling rate was 50° C/min, after a 30 minutes annealing period in the same atmosphere. The sample surface size is $5 \times 5 \text{ mm}^2$.

* Correspondence at rebolini@ill.fr

† Deceased

B. Instrument details

1. The initial characterization of the film was performed with Transmission Electron Microscopy (TEM) using an ARM200F (double corrected JEOL TEM, 200 kV) microscope with z dependent contrast images at the CRISMAT laboratory in Caen (France).
2. The X-ray diffraction (XRD) measurements were carried out using the SmartLab Rigaku diffractometer (CEA-CNRS, Grenoble, France). The diffractometer is equipped with a standard Cu anode source, with optional double bounce Ge (220) monochromator. The detector is a NaI scintillation point detector. The reflections were measured using Cu $K_{\alpha 1}$ radiation ($\lambda = 1.5406 \text{ \AA}$). The resolution and beam size at sample were selected using appropriate Soller slits, on both incident and receiving sides. The primary beam size was 0.4 mm (vertical) \times 12 mm (horizontal).
3. The magnetic characterization of the film was performed using an XL Quantum Design SQUID magnetometer at Institut Néel, Grenoble (France).
4. Finally, single crystal neutron diffraction (ND) experiments were performed on the the D10/D10+ instrument at the Institute Laue-Langevin (Grenoble, France). D10 was used in the four-circle mode, equipped with a Eulerian cradle and a He-flow cryostat. The optional energy analysis mode was used in order to reduce the inelastic signal coming from the substrate. An incident wavelength of 2.36 \AA was selected using a pyrolytic graphite monochromator, and an ^3He point detector was used to collect the data. The magnetic structure was further analyzed using the upgraded D10+ instrument.

III. NUCLEAR STRUCTURE DETERMINATION

Figure 1(a) shows a TEM image of the sample, seen along $[010]$ direction, in the STO unit cell (which is cubic with $a = b = c = 3.9 \text{ \AA}$). There are two domains of STO, as expected from the deposition mechanism. The stacking of layers along the c-axis (out-of-plane direction) shows the quality of the film epitaxy. The thickness of the LSMO film is determined to be 40.9 nm . A very thin layer (4 nm) of silicon oxide formed in-between the substrate (Si) and STO.

In electron diffraction experiment (cf. Appendix A), the observation of Bragg peaks at $1/\sqrt{2} a_{\text{STO}}^*$ (in-plane), and at $1/2 c_{\text{STO}}^*$ (out-of-plane) in the paramagnetic phase, requires a doubling of the LSMO-film unit cell compared to the STO and the ideal-perovskite bulk-LSMO ones (see Fig. 1(b) for schematic representation). This results in LSMO in-plane lattice axes being rotated by 45° compared to the STO ones, associated with a doubling in the out-of-plane direction as well ($\vec{a}_{\text{LSMO}} = \vec{a}_{\text{STO}} + \vec{b}_{\text{STO}}$, $\vec{b}_{\text{LSMO}} = -\vec{a}_{\text{STO}} + \vec{b}_{\text{STO}}$, $\vec{c}_{\text{LSMO}} = 2\vec{c}_{\text{STO}}$). Henceforth, we will describe the LSMO film in this doubled unit cell.

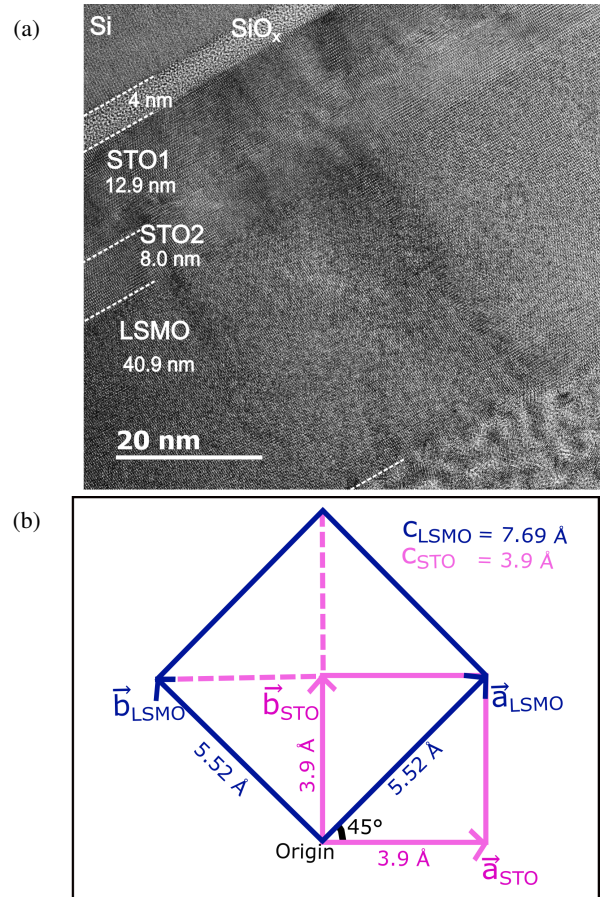


FIG. 1. (a) TEM image of the LSMO thin film seen along $[010]$ direction in STO unit cell. (b) Relationship between STO and LSMO unit cells.

Further insights into the crystal structure of the film were obtained using XRD measurements at room temperature, showing that the nuclear structure of the film follows the $I4/m$ space-group symmetry. The lattice parameters of the body-centered cell, obtained from various XRD peak positions — (00ℓ) and $(hk0)$ families — are: $a_{\text{LSMO}} = b_{\text{LSMO}} = 5.522(6) \text{ \AA}$ and $c_{\text{LSMO}} = 7.690(4) \text{ \AA}$. The a and b lattice constants of LSMO and STO are found to be exactly related $a_{\text{LSMO}} = \sqrt{2} a_{\text{STO}}$, which confirms that the film is constrained by the STO layer despite the presence of a thin buffer of silicon oxide. An $\omega - 2\theta$ scan performed along (00ℓ) film direction, is shown in Figure 2(a). The strongest peak is $(004)_{\text{Si}}$ from the Si substrate. The $(002)_{\text{LSMO}}$, $(004)_{\text{LSMO}}$, $(006)_{\text{LSMO}}$, and $(008)_{\text{LSMO}}$ Bragg reflections of the LSMO film can be seen clearly. The peaks from the STO layer are very close to the film peaks, but can be distinguished for the (002) and (004) reflections, thanks to the small thickness of the STO buffer layer. This confirms that the growth of the film is along c-axis for both STO and LSMO.

The in-plane reflections ($\ell = 0$) of the STO and LSMO were found in complete overlap. This reaffirms the fact that the film and the STO layer follow the same constraints and in-plane symmetry. In addition, Figure 2(b) shows a cut of the 2D scans along ϕ , corresponding to the maximum of the

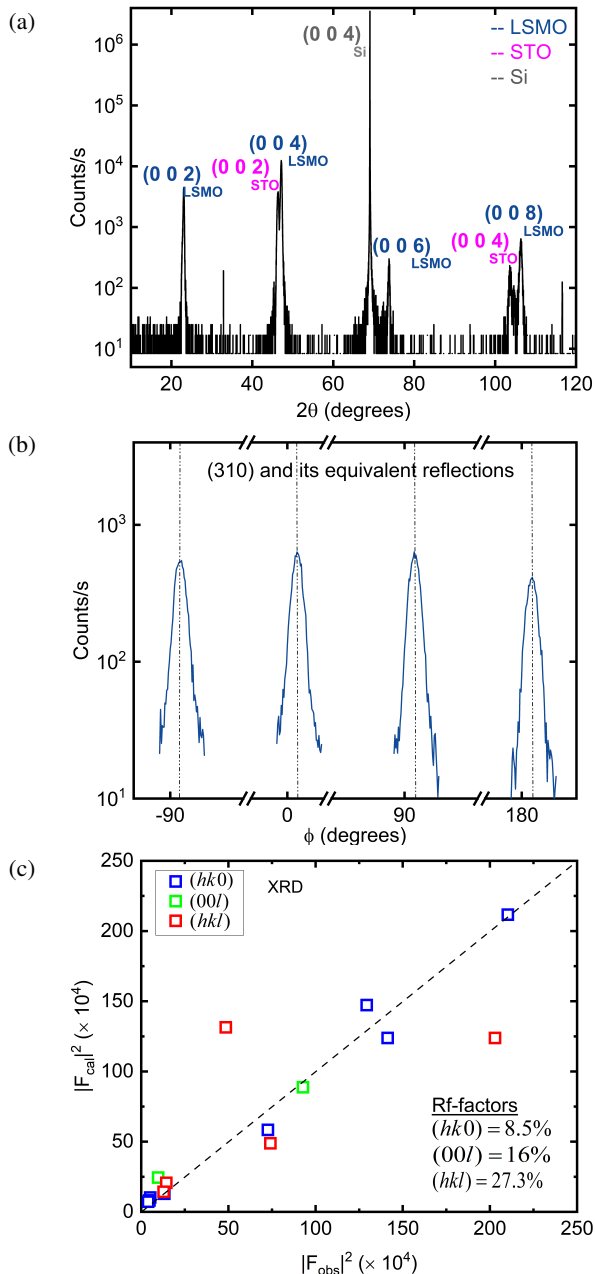


FIG. 2. XRD measurements: (a) $\omega - 2\theta$ scan along (00l) depicting peaks from Si (substrate), STO (buffer layer) and LSMO (thin film). The intensity is presented on \log_{10} scale. (b) 1D cut of the 2D $\phi - 2\theta$ (detector-sample rotation) scans of the $(310)_{\text{LSMO}}$ peak and its equivalent reflections. There is complete overlap of LSMO and STO peaks for such in-plane reflections. The intensity is presented on \log_{10} scale. (c) Comparison of the observed structure factors with the calculated ones for the $I4/m$ space group.

$(310)_{\text{LSMO}}$ peak. These well-centered equivalent peaks at consecutive 90° rotation of the sample indicate the presence of an in-plane 4-fold symmetry in the film.

In total, 56 reflections (15 independent) were measured using two different instrumental set-ups: in-plane and out-of-plane. Several corrections were applied to the measured

TABLE I. Atomic positions and Wyckoff sites of the LSMO film in the $I4/m$ space group ($a=b=5.52$ Å, $c=7.69$ Å).

Atom	Wyckoff site	Fractional coordinates
Mn1	2a	(0, 0, 0)
Mn2	2b	(0, 0, 1/2)
La/Sr	4d	(0, 1/2, 1/4)
O1	4e	(0, 0, 1/4)
O2	8h	(1/4, 1/4, 0)

counts/s, namely the normalization with respect to film area under diffraction, the Lorentz factor and the polarization [24]. The integrated intensities were calculated by performing numerical addition of counts/s using a homemade python script (cf. supplementary material).

The refinement of the nuclear structure was performed with the FullProf package [25], using least-square fitting to compare observed and calculated structure factors. The reliability of the fit was measured using Rf-factor [26]. The data were divided into 3 sets ($hk0$), $(00l)$, and the general one (hkl), which were refined separately as we used different experimental set-ups. In the $I4/m$ (No. 79) space-group, the obtained Rf-factors are: $\text{Rf-}(hk0) = 8.5\%$, $\text{Rf-}(00l) = 16\%$, $\text{Rf-general} = 27.3\%$. Figure 2(c) shows the comparison between the squares of calculated and observed structure factors ($|F_{\text{calc}}|^2$ and $|F_{\text{obs}}|^2$) for different reflections. The relatively high value of Rf-general can be attributed to a combination of the La/Sr disorder present in the system and the strain-relaxation of the film. This is argued because the out-of-plane peaks are asymmetric, with a long tail on the small 2θ side, indicating increase in the c lattice parameter (cf. supplementary material).

Due to limited number of measured reflections, it is important to note that only the scale factors were refined during the fitting process. Removing the mirror plane perpendicular to the c -axis ($I4$ space group) gives the possibility to optimize the z -positions of all the atoms, but the refinement is unstable due to the too-large number of parameters. To overcome this problem, we ran a 3D loop varying the z -positions of atoms and rotating the in-plane oxygen octahedra through a homemade Python script with the FullProf software. It was found that the minima of the 3 Rf-factors is at negligible distortions from the original structure. There is therefore no indication that the mirror plane is absent and hence, the best possible fit of the nuclear structure data is with $I4/m$ space group. The atomic positions are provided in Table I. One should however remember that the resolution of such XRD measurements on thin films is not good-enough to identify small distortions possibly leading to a symmetry breaking.

IV. MAGNETIC STRUCTURE DETERMINATION

A. SQUID

Macroscopic magnetic properties of the film were investigated by performing SQUID measurements in various ap-

plied magnetic fields, over a wide range of temperature. We first measured the susceptibility in the paramagnetic phase and found it very small. Since the Si susceptibility is known to be temperature independent, the magnetic contribution of the substrate can be considered as negligible in a 0.3 T field. Figure 3(a) shows the magnetization measured as a function of increasing temperature, after cooling in an in-plane 0.25 T field. The two curves (in the absence of field and under an applied field of 0.25 T) clearly show the magnetic ordering transition at 260 K.

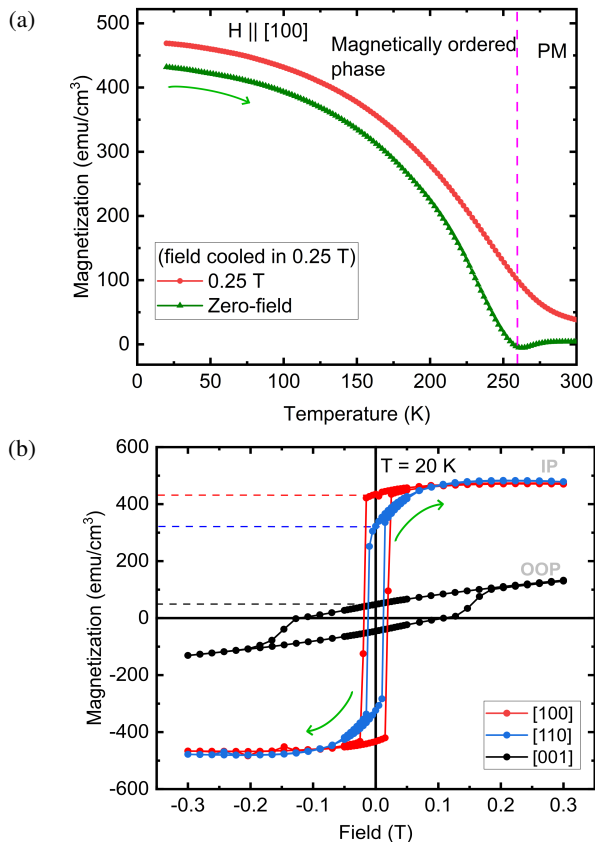


FIG. 3. SQUID magnetic measurements: (a) Temperature dependence of magnetization for applied field along in-plane [100], in 0.25 T and zero-field (field cooled). The dashed line near 260 K marks the transition from paramagnetic (PM) to magnetically ordered phase. (b) Magnetic hysteresis loops at 20 K for field applied up to 0.3 T along [100], [110] and [001] film directions.

Figure 3(b) shows the magnetic hysteresis at 20 K along the 3 film directions: [100], [110], and [001]. The moments along the [100] direction saturate in a ≈ 0.1 T field. The coercive field (H_c) is 0.02 T, indicating a soft magnetic nature. The shape of the hysteresis shows that the moments switch from the [100] to the $[\bar{1}00]$ direction instantaneously, when a field equal to H_c is applied in the reverse direction. Such a behavior is typical from a mono-domain ferromagnetic (FM) spin arrangement. The [110] hysteresis loop exhibits the same saturation and instantaneous switching as the [100] one, while H_c is about half (0.01 T). The spontaneous magnetization in the [100] direction (μ_a) is very close to its saturation value, indi-

ating that [100] is the easy-axis direction. The fact that the spontaneous magnetization in the [110] direction is $1/\sqrt{2} \mu_a$ can be interpreted as a rotation of the moments from the applied field direction toward the easy-axis direction, when the field along [110] is reduced below 0.1 T. The slope in the region from 0 to 0.1 T (blue curve in Figure 3(b)) is the result of this moment rotation.

The out-of-plane hysteresis behavior is slightly different. The moments are not saturated at 0.3 T and H_c is higher (≈ 0.13 T), suggesting a strong magnetic anisotropy. Ultimately, the moments are completely aligned along [001] in a field of ≈ 2 T (see supplementary material). When the applied field is reduced to zero, the non-zero magnetization along [001] shows that the moments are not completely in-plane but have an out-of-plane component (μ_c) (see Fig. 3(b)). The ratio between μ_c and μ_a is about 0.1, meaning that the out-of-plane tilt of the moments is small. Unlike in-plane, the out-of-plane hysteresis loops shows that the moments switch from the [001] to the $[00\bar{1}]$ direction in a continuous, linear way.

From these observations, one can deduce that the moments components in zero field are $(\mu_a, 0, \mu_c)$, the [100] in-plane components being ferromagnetically aligned. Based on the shape of out-of-plane hysteresis curves, two different scenarios can be proposed. Either the moments are ordered anti-ferromagnetically along the \vec{c} axis, with a small uncompensated magnetization of the $2a$ and $2b$ sites given by the μ_c/μ_a ratio, or the system is completely FM in nature with moment $(\mu_a, 0, \mu_c)$. Let us note here that a magnetic moment with both an in-plane and out-of plane component is incompatible with magnetic atoms located at a crystallographic site with a rotation axis along \vec{c} , as the $2a$ and $2b$ Mn Wyckoff-sites of the $I4/m$ group, obtained from room temperature XRD (see Table I).

B. Neutron diffraction

In order to distinguish between these two models and determine the moment size, single crystal ND measurements were performed. The film was aligned using the substrate Si peak positions and several reflections were measured using $\omega - 2\theta$ and ω scans. All the measured peaks were integrated using Gaussian function fitting. The lattice parameters obtained from ND at 300 K are as follows: $a_{\text{LSMO}} = b_{\text{LSMO}} = 5.51 \pm 0.04$ Å and $c_{\text{LSMO}} = 7.71 \pm 0.02$ Å. These values are in good agreement with the XRD results.

The peaks measured at 300 K (paramagnetic phase of the LSMO film) were fitted with the $I4/m$ nuclear space group using FullProf. The comparison of the observed and calculated structure factors is shown in Figure 4(a). For the nuclear data, only the scale factor was refined and it is in agreement with the $I4/m$ space group (Rf-factor = 10.4%). The temperature dependence of a few peaks intensities was followed in the range 20 - 300 K using $\omega - 2\theta$ scans. The magnetic intensity appears on existing reflexions and is responsible for the peaks increase below 250 K. As a consequence the long-range magnetic ordering propagation vector is $\vec{q} = (000)$. The magnetic contribution is shown for the (202) reflection in Figure 4(b)

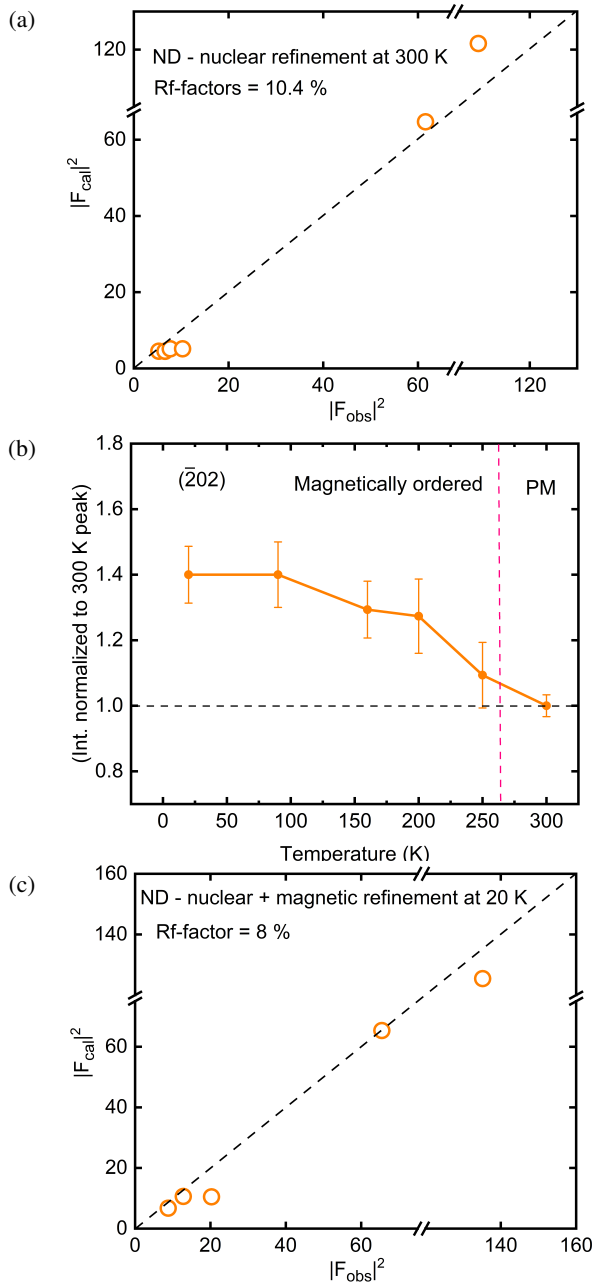


FIG. 4. Single crystal neutron diffraction measurements using D10. (a) Fit of the nuclear data at 300 K with $I4/m$ space group. (b) Temperature dependence of the integrated intensity of the $(\bar{2}02)$ peak, in the range 20 - 300 K, measured using $\omega - 2\theta$ scans. (c) Fit of the ND data at 20 K with nuclear and magnetic refinement.

and is consistent with the SQUID results discussed above.

From SQUID measurements, we know that the in-plane moments are aligned ferromagnetically but need to establish the out-of-plane ordering using ND. An initial set of 5 reflections (containing both nuclear and magnetic contributions) was measured on D10 in the magnetically ordered phase, at 20 K. Unfortunately, this set was not enough to answer the out-of-plane coupling question. Measurement of some extra reflections became possible thanks to the upgrade of D10 into

D10+. On D10+, we measured peaks with pure magnetic content, that are absent for an FM structure. The set includes the (201), (111) and (101) peaks. Our theoretical magnetic intensity calculations (using FullProf) showed that these peaks should be sufficient to distinguish between different antiferromagnetic (AFM) models on the out-of-plane component.

Figure 5(a) displays the (002) peak measured at 300 K with both D10 and D10+, with normalized measurement time. As can be clearly seen, the D10+ upgrade provides a large increase in intensity (~ 2.5). This is a remarkable achievement, that will allow significant improvements to studies like this one where we need information on weak peaks. This is particularly important as we did not detect any intensity on the set of peaks selected to decipher the AFM ordering of the moment out-of-plane component. The $(\bar{2}0\bar{1})$ reflection is shown as matter of example on Fig. 5(b). We can thus conclude that the ordering is completely FM in nature.

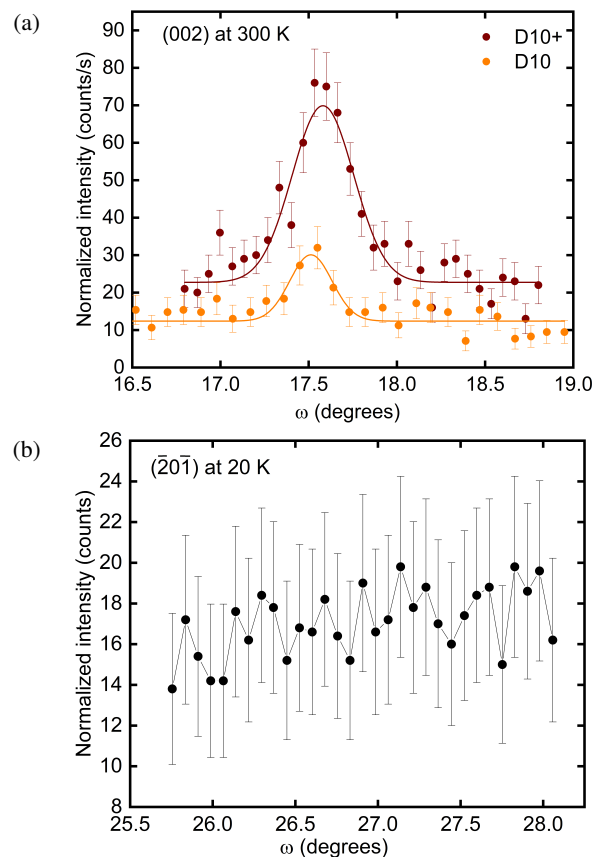


FIG. 5. Single-crystal neutron diffraction measurement on ILL-D10+. (a) Comparison of the (002) peak intensities at 300 K, measured using D10 and upgraded D10+. (b) Purely magnetic AFM $(\bar{2}0\bar{1})$ measured at 20 K.

The μ_a and μ_c components of the moments were then evaluated by the fitting of the 20 K data-set in FullProf. Since the \vec{a} and \vec{b} axes are supposed to be equivalent in the film, two magnetic domains $(\mu_a, 0, \mu_c)$ and $(0, \mu_a, \mu_c)$ were used with 50 % occupancy. In the magnetic refinement, the nuclear structure was described in the $P\bar{1}$ space group (see Appendix

B for detailed symmetry analysis) and the scale factor taken from the 300 K data. The μ_a/μ_c ratio was optimized while keeping the norm of the moment fixed at its theoretical value of $3.7 \mu_B$ per Mn ($0.67\mu_{\text{Mn}^{3+}} + 0.33\mu_{\text{Mn}^{4+}}$). While it was not possible to accurately determine the ratio, the best Rf-factor was for $0.1 \leq \mu_a/\mu_c \leq 0.3$, in agreement with the SQUID experiment. The SQUID $\mu_c/\mu_a = 0.1$ ratio gives an Rf-factor of 8% as shown in Figure 4(c). The Mn moment for this model is $(3.5, 0, 0.3)\mu_B$. It corresponds to an out-of-plane tilt of $\simeq 6^\circ$. Let us remember that in bulk LSMO, the magnetic order is also FM, but the easy-axis is along $[111]$ [27], whereas in ultra-thin films, less than 3 nm thick, there is a co-existence of FM and AFM phases [16, 28]. In this regard, we can say that our film, with a 40.9 nm thickness, is in an intermediate regime, not fully constrained, but not yet fully relaxed.

C. Symmetry analysis

Symmetry analysis shows that the resolved magnetic structure is not compatible with the $I4/m$ crystallographic group. In fact such a FM arrangement of moments, with both in-plane and out-of-plane components, is only compatible with the $P\bar{1}$ space group ($P\bar{1}'$ magnetic group) with Mn at any Wyckoff site (see Appendix B for detailed calculations). By continuity with the $I4/m$ group found in XRD we can use a $I\bar{1}'$ group with the Mn atoms in $2a$ and $2b$. It is clear here that diffraction techniques do not provide data of high-enough quality on such thin films, to detect small distortions in the structure and thus weak symmetry breaking.

V. CONCLUSION

In summary, we synthesized a high quality epitaxial LSMO thin-film 40.9 nm thick, on a Si substrate, with a buffer layer of STO. The thin thickness of the buffer layer allowed us to distinguish the film diffraction peaks from those of STO. We showed that single crystal diffraction measurements can be performed on such highly epitaxial films using both X-rays and neutrons. The 300 K nuclear structure was refined in the $I4/m$ space group using XRD data, and corroborated using the neutron diffraction ones. Below 260 K the film undergoes a paramagnetic to ferromagnetic transition, the magnetic structure being resolved using a combination of SQUID and ND measurements. The Mn magnetic moment were found to have an essentially in-plane orientation but a weak out-of-plane component and were refined to be $(3.5, 0, 0.3)\mu_B$. Considering the fact that the bulk magnetic moments are along the $[111]$ direction and that very-thin films present a coexistence of FM and AFM phases, one can speculate that at such thickness we are in the regime where the in-plane symmetry constraints imposed by the substrate start to relax [29], while the in-plane unit-cell lengths are still frozen. One can also think that the amplitude of the moment out-of-plane component can be controlled by the film thickness, and that at a somewhat thinner thickness one may have FM films, with fully in-plane magnetic moments and $I4/m$ symmetry.

Such studies combining X-Ray and neutron diffraction, SQUID measurements and symmetry analysis allow considerable insight into the structural and magnetic properties of very thin films.

The authors have no conflicts to disclose.

The data that support the findings of this study are available from the corresponding author upon reasonable request and will be available from data.i11.eu at <https://doi.i11.fr/10.5291/ILL-DATA.5-54-371> after an embargo period of 3 years.

Appendix A: Electron diffraction results: doubling of the unit cell

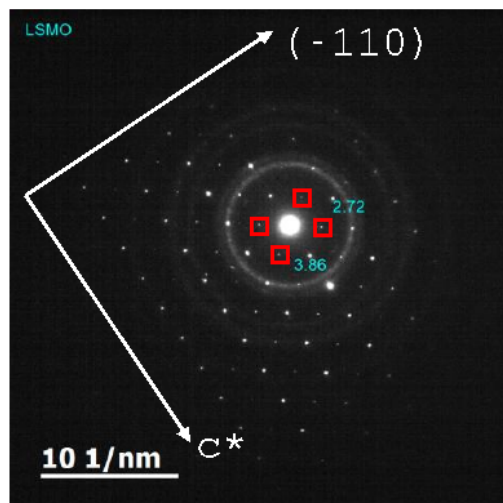


FIG. 6. Electron diffraction peaks measured on the LSMO film. Red squares highlight the peaks requiring a unit cell increase (direction (-110) and c^* are in the STO unit-cell notations)

Figure 6 displays the LSMO film electron diffraction peaks in the reciprocal space labeled in the STO basis set. The peaks with the smallest components along each directions (squared in red on the figure) correspond to

$$\pm(-1/2, 1/2, \pm 1/2)_{\text{STO}}$$

as $2.72 \text{ \AA} = 1/\sqrt{2} a_{\text{STO}}$. The existence of such a diffraction peak in the paramagnetic phase directly requires a doubling of the LSMO film unit cell both the in-plane and out-of-plane, as compared to the STO one. It results for the LSMO film lattice parameter

$$\vec{a}_{\text{LSMO}} = \vec{a}_{\text{STO}} + \vec{b}_{\text{STO}} \quad (\text{A1})$$

$$\vec{b}_{\text{LSMO}} = -\vec{a}_{\text{STO}} + \vec{b}_{\text{STO}} \quad (\text{A2})$$

$$\vec{c}_{\text{LSMO}} = 2\vec{c}_{\text{STO}} \quad (\text{A3})$$

Appendix B: Space group symmetry analysis

We have shown that the Mn magnetic moments have both an in-plane and an out-of-plane component.

Group theory tells us that a magnetic atom, located on a site with a rotation axis (or on a mirror plane), can only have a magnetic moment either along this axis or in the perpendicular plane (either in the plane or along the perpendicular axis). As a result the Mn atoms of the film cannot be located at a Wyckoff site with a rotation around the \bar{c} axis or a mirror plane perpendicular to the latter. This simple statement strongly constrain the possible space groups of the film.

Indeed in the paramagnetic phase space group : $I4/m$, the Mn atoms can be located either on a Wyckoff's site of 4 degeneracy ($4c$, $4d$, $4e$, $4f$) or on two Wyckoff's of degeneracy 2 ($2a$ and $2b$). All those sites however have a two- or four-fold rotation axis along \bar{c} (see Table II), invalidating $I4/m$ as a possible LSMO space group for the magnetic phase.

Keeping the I centering the subgroups of $I4/m$ with $k_{\text{index}} = 1$ are $\bar{I}4$, $I4$, $I2/m$, Im , $I2$, they other one being only $P\bar{I}$ and $P1$. Again, one can easily see from Table II that the only possibilities compatible with the existence of both an in-plane and out-of-plane component of the magnetization are $I2/m$ with the Mn ions at the $4e$ or $4f$ locations, the $I2$ with the Mn ions at the $4c$ location or the Im with the Mn ions at the $4b$ location.

TABLE II. Different possible Wyckoff's sites for the Mn atom, in the $I4/m$ group and its subgroups keeping the body-centered unit cell.

SG	Possible Mn Wyckoff's site	Site symmetry	SG	Possible Mn Wyckoff's site	Site symmetry
$I4/m$	$2a + 2b$	$\dots 4/m$	$I2/m$	$2a + 2b$	$\dots 2/m$
	$4c$	$\dots 2/m$		$2c + 2d$	$\dots 2/m$
	$4d$	$\dots 4$		$4e$	-1
	$4e$	$\dots 4$		$4f$	-1
$\bar{I}4$	$2a + 2b$	$\dots 4$	$I2$	$4g$	$\dots 2$
	$2c + 2d$	$\dots 4$		$4h$	$\dots 2$
$I4$	$4e$	$\dots 2$	Im	$4i$	$\dots m$
	$4f$	$\dots 2$		$2a + 2b$	$\dots 2$
	$2a + 2a$	$\dots 4$		$4c$	1
	$4b$	$\dots 2$		$2a + 2a$	$\dots m$
				$4b$	1

Let us thus analyze those possibilities in view of the neutrons scattering results.

1. Mn on $4e$ or $4f$ sites in the $I2/m'$ magnetic group

The magnetic space group associated with the $I2/m$ crystallographic group is $I2/m'$ if one considers that only the CPT(= i') symmetry operation is respected in our space-time.

The symmetry operations of the $I112/m'$ groups thus transform the atoms and their magnetic moment has follows

Sym. Op.	Frac. atom. coord.			Magn. moment		
1	x	y	z	μ_x	μ_y	μ_z
$2_{0,0,z}$	$-x$	$-y$	z	$-\mu_x$	$-\mu_y$	μ_z
\bar{I}'	$-x$	$-y$	$-z$	$-\mu_x$	$-\mu_y$	$-\mu_z$
m'	x	y	$-z$	μ_x	μ_y	$-\mu_z$
$t_{(\frac{1}{2}, \frac{1}{2}, 0)}$	$x + \frac{1}{2}$	$y + \frac{1}{2}$	$z + \frac{1}{2}$	μ_x	μ_y	μ_z
$t \circ 2_{0,0,z}$	$-x + \frac{1}{2}$	$-y + \frac{1}{2}$	$z + \frac{1}{2}$	$-\mu_x$	$-\mu_y$	μ_z
$t \circ \bar{I}'$	$-x + \frac{1}{2}$	$-y + \frac{1}{2}$	$-z + \frac{1}{2}$	$-\mu_x$	$-\mu_y$	$-\mu_z$
$t \circ m'$	$x + \frac{1}{2}$	$y + \frac{1}{2}$	$-z + \frac{1}{2}$	μ_x	μ_y	$-\mu_z$

TABLE III. Action of the symmetry operations in the $I2/m'$ group.

The $4e$ Wyckoff's sites correspond to $(1/4, 1/4, 1/4)$, $(3/4, 3/4, 1/4)$, $(3/4, 3/4, 3/4)$ and $(1/4, 1/4, 3/4)$. They are thus invariant under the $t \circ \bar{I}'$ transformation, as should be their magnetic moment. This provides conditions for the irreducible representation (irrep) to which the magnetic structure belongs ; indeed it has to have a -1 character on the $t \circ \bar{I}'$ symmetry operation. This is the case for the A_u , B_u where the \bar{I}' symmetry operation is associated with a -1 character, and the A'_g and B'_g irreps where it is the partial translation $t_{(\frac{1}{2}, \frac{1}{2}, 0)}$ that is associated with a -1 character.

Irrep	Frac. atom. coord.			Magn. moment		
A_u	$1/4$	$1/4$	$1/4$	μ_x	μ_y	μ_z
	$3/4$	$3/4$	$1/4$	$-\mu_x$	$-\mu_y$	μ_z
	$3/4$	$3/4$	$3/4$	μ_x	μ_y	μ_z
	$1/4$	$1/4$	$3/4$	$-\mu_x$	$-\mu_y$	μ_z
B_u	$1/4$	$1/4$	$1/4$	μ_x	μ_y	μ_z
	$3/4$	$3/4$	$1/4$	μ_x	μ_y	$-\mu_z$
	$3/4$	$3/4$	$3/4$	μ_x	μ_y	μ_z
	$1/4$	$1/4$	$3/4$	μ_x	μ_y	$-\mu_z$
A'_g	$1/4$	$1/4$	$1/4$	μ_x	μ_y	μ_z
	$3/4$	$3/4$	$1/4$	$-\mu_x$	$-\mu_y$	μ_z
	$3/4$	$3/4$	$3/4$	$-\mu_x$	$-\mu_y$	$-\mu_z$
	$1/4$	$1/4$	$3/4$	μ_x	μ_y	$-\mu_z$
B'_g	$1/4$	$1/4$	$1/4$	μ_x	μ_y	μ_z
	$3/4$	$3/4$	$1/4$	μ_x	μ_y	$-\mu_z$
	$3/4$	$3/4$	$3/4$	$-\mu_x$	$-\mu_y$	$-\mu_z$
	$1/4$	$1/4$	$3/4$	$-\mu_x$	$-\mu_y$	μ_z

TABLE IV. Magnetic moment associated with the possible irreps for the $4e$ Mn sites in the $I2/m'$ group.

One sees immediately from Table IV that none of the allowed irreps are associated with the FM ordering found in neutron diffraction and SQUID experiments. Indeed, according to Table IV, a FM ordering would require either pure in-plane or pure out-of-plane magnetic moments, while both those hypotheses are incompatible with the experimental results.

The $4f$ exhibit a behavior similar to the $4e$ one. As a consequence the $I2/m$ crystallographic group cannot be the film space group and one has to consider the other alternatives.

2. Mn on 4c sites in the $I2$ magnetic group

The magnetic space group associated with the $I2$ crystallographic group is $I2$ if one considers that only the CPT(= i') symmetry operation is respected in our space-time.

The symmetry operations of the $I112$ group thus transform the atoms and their magnetic moment as follows

Sym. Op.	Frac. atom. coord.			Magn. moment		
1	x	y	z	μ_x	μ_y	μ_z
$2_{0,0,z}$	$-x$	$-y$	z	$-\mu_x$	$-\mu_y$	μ_z
$t_{(\frac{1}{2}, \frac{1}{2}, 0)}$	$x + \frac{1}{2}$	$y + \frac{1}{2}$	$z + \frac{1}{2}$	μ_x	μ_y	μ_z
$t \circ 2_{0,0,z}$	$-x + \frac{1}{2}$	$-y + \frac{1}{2}$	$z + \frac{1}{2}$	$-\mu_x$	$-\mu_y$	μ_z

TABLE V. Action of the symmetry operations in the $I2$ group.

The 4c Wickoff's sites correspond to $(1/4, 1/4, 1/4)$, $(3/4, 3/4, 1/4)$, $(3/4, 3/4, 3/4)$ and $(1/4, 1/4, 3/4)$. There are four irreps in this group (see Table VI), but it is easy to see that a FM ordering is again incompatible in this group with magnetic moment with both in-plane and out-of-plane components.

$I2$	E	$2_{0,0,z}$	$t_{(\frac{1}{2}, \frac{1}{2}, 0)}$	$t \circ 2_{0,0,z}$
A	1	1	1	1
B	1	-1	1	-1
A'	1	1	-1	-1
B'	1	-1	-1	1

TABLE VI. Character table of the $I2$ group.

Let us see the next hypothesis.

3. Mn on 4b sites in the Im magnetic group

The magnetic space group associated with the Im crystallographic group is Im' if one considers that only the CPT(= i') symmetry operation is respected in our space-time.

The symmetry operations of the $I11m'$ group thus transform the atoms and their magnetic moment as follows

Sym. Op.	Frac. atom. coord.			Magn. moment		
1	x	y	z	μ_x	μ_y	μ_z
m'	x	y	$-z$	μ_x	μ_y	$-\mu_z$
$t_{(\frac{1}{2}, \frac{1}{2}, 0)}$	$x + \frac{1}{2}$	$y + \frac{1}{2}$	$z + \frac{1}{2}$	μ_x	μ_y	μ_z
$t \circ m'$	$x + \frac{1}{2}$	$y + \frac{1}{2}$	$-z + \frac{1}{2}$	μ_x	μ_y	$-\mu_z$

TABLE VII. Action of the symmetry operations in the Im' group.

The 4b Wickoff's sites correspond to $(1/4, 1/4, 1/4)$, $(1/4, 1/4, 3/4)$, $(3/4, 3/4, 3/4)$ and $(3/4, 3/4, 1/4)$. There are four irreps in this group (see Table VIII), but it is easy to see that a FM ordering is again incompatible with magnetic moment with both in-plane and out-of-plane components.

$I2$	E	m'	$t_{(\frac{1}{2}, \frac{1}{2}, 0)}$	$t \circ m'$
A	1	1	1	1
B	1	-1	1	-1
A'	1	1	-1	-1
B'	1	-1	-1	1

TABLE VIII. Character table of the Im' group.

4. Conclusion on symmetry analysis

At this stage the $I4/m$, $I2/m$, $I2$ and Im crystallographic groups have been out-ruled by the magnetic structure found in neutrons scattering and SQUID measurements. The only possibility within the same unit cell is the $P\bar{1}$ or $P1$ groups.

The magnetic groups associated with $P\bar{1}$ is $P\bar{1}'$. It transform the magnetic moments as follow

Sym. Op.	Frac. atom. coord.			Magn. moment		
1	x	y	z	μ_x	μ_y	μ_z
i'	$-x$	$-y$	$-z$	$-\mu_x$	$-\mu_y$	$-\mu_z$

TABLE IX. Action of the symmetry operations in the $P\bar{1}'$ group.

The Mn atoms must now be in two independent $2i$ Wickoff's positions, that is $(1/4, 1/4, 1/4)$, $(3/4, 3/4, 3/4)$ for the first one and $(1/4, 1/4, 3/4)$, $(3/4, 3/4, 1/4)$ for the second one. One can now see that a FM order correspond to the B irrep and that both in-plane and out-of-plane components are allowed.

$P\bar{1}'$	E	i'
A	1	1
B	1	-1

TABLE X. Character table of the $P\bar{1}'$ group.

One can thus conclude that among the $I4/m'$ sub-groups only the $P\bar{1}'$ group is compatible with the FM ordering found in our experimental results.

[1] G. H. Jonker and J. H. Van Santen, Physica **16**, 337 (1950).

[2] C. W. Searle and S. T. Wang, Canadian Journal of Physics **47**,

- 2703 (1969).
- [3] Y. Tokura, A. Urushibara, Y. Moritomo, T. Arima, A. Asamitsu, G. Kido, and N. Furukawa, *Journal of the Physical Society of Japan* **63**, 3931 (1994).
- [4] P. Schiffer, A. P. Ramirez, W. Bao, and S. W. Cheong, *Physical Review Letters* **75**, 3336 (1995).
- [5] A. Urushibara, Y. Moritomo, T. Arima, A. Asamitsu, G. Kido, and Y. Tokura, *Phys. Rev. B* **51**, 14103 (1995).
- [6] S. J. Hibble, S. P. Cooper, A. C. Hannon, I. D. Fawcett, and M. Greenblatt, *Journal of Physics: Condensed Matter* **11**, 9221 (1999).
- [7] C. Zener, *Phys. Rev.* **82**, 403 (1951).
- [8] A. J. Millis, B. I. Shraiman, and R. Mueller, *Physical Review Letters* **77**, 175 (1996).
- [9] C. Zener, Interaction between the *d*-shells in the transition metals. ii. ferromagnetic compounds of manganese with perovskite structure, *Phys. Rev.* **82**, 403 (1951).
- [10] J.-H. Park, E. Vescovo, H.-J. Kim, C. Kwon, R. Ramesh, and T. Venkatesan, *NATURE* **392**, 794 (1998).
- [11] J. M. De Teresa, A. Barthélemy, A. Fert, J. P. Contour, F. Montaigne, and P. Seneor, *Science (New York, N.Y.)* **286**, 507 (1999).
- [12] H. L. Ju, C. Kwon, Q. Li, R. L. Greene, and T. Venkatesan, *Applied Physics Letters* **65**, 2108 (1994).
- [13] J. Z. Sun, D. W. Abraham, and R. A. Rao, *Appl. Phys. Lett* **74**, 3017 (1999).
- [14] F. Tsui, M. C. Smoak, and T. K. Nath, *Appl. Phys. Lett* **76**, 2421 (2000).
- [15] M. Huijben, L. W. Martin, Y. H. Chu, M. B. Holcomb, P. Yu, G. Rijnders, D. H. Blank, and R. Ramesh, *Physical Review B - Condensed Matter and Materials Physics* **78**, 094413 (2008).
- [16] A. K. Pradhan, D. Hunter, T. Williams, B. Lasley-Hunter, R. Bah, H. Mustafa, R. Rakhimov, J. Zhang, D. J. Sellmyer, E. E. Carpenter, D. R. Sahu, and J.-L. Huang, *Journal of Applied Physics* **103**, 023914 (2008).
- [17] C. Ma, Z. Yang, and S. Picozzi, *Journal of Physics: Condensed Matter* **18**, 7717 (2006).
- [18] R. Herger, P. R. Willmott, C. M. Schlepütz, M. Björck, S. A. Pauli, D. Martocchia, B. D. Patterson, D. Kumah, R. Clarke, Y. Yacoby, and M. Döbeli, *Phys. Rev. B* **77**, 085401 (2008).
- [19] C. Aruta, G. Ghiringhelli, V. Bisogni, L. Braicovich, N. B. Brookes, A. Tebano, and G. Balestrino, *Phys. Rev. B* **80**, 014431 (2009).
- [20] A. Vailionis, H. Boschker, Z. Liao, J. R. Smit, G. Rijnders, M. Huijben, and G. Koster, *Applied Physics Letters* **105**, 131906 (2014).
- [21] Z. Liao, F. Li, P. Gao, L. Li, J. Guo, X. Pan, R. Jin, E. W. Plummer, and J. Zhang, *Phys. Rev. B* **92**, 125123 (2015).
- [22] Å. Monsen, J. E. Boschker, F. Macià, J. W. Wells, P. Nordblad, A. D. Kent, R. Mathieu, T. Tybell, and E. Wahlström, *Journal of Magnetism and Magnetic Materials* **369**, 197 (2014).
- [23] L. Chen, Z. Wang, G. Wang, H. Guo, M. Saghayezhian, Z. Liao, Y. Zhu, E. W. Plummer, and J. Zhang, *Phys. Rev. Mater.* **3**, 044407 (2019).
- [24] M. J. Bueger and G. E. Klein, *Journal of Applied Physics* **16**, 408 (1945).
- [25] J. Rodríguez-Carvajal, *Physica B: Condensed Matter* **192**, 55 (1993).
- [26] H. M. Rietveld, *Journal of Applied Crystallography* **2**, 65 (1969).
- [27] G. Jonker and J. Van Santen, Ferromagnetic compounds of manganese with perovskite structure, *Physica* **16**, 337 (1950).
- [28] H. Chen, Y. Yu, Z. Wang, Y. Bai, H. Lin, X. Li, H. Liu, T. Miao, Y. Kou, Y. Zhang, Y. Li, J. Tang, Z. Wang, P. Cai, Y. Zhu, Z. Cheng, X. Zhong, W. Wang, X. Gao, L. Yin, R. Wu, and J. Shen, *Phys. Rev. B* **99**, 214419 (2019).
- [29] M.-B. Lepetit, B. Mercey, and C. Simon, Interface effects in perovskite thin films, *Phys. Rev. Lett.* **108**, 087202 (2012).

Nuclear and magnetic structure of an epitaxial $\text{La}_{0.67}\text{Sr}_{0.33}\text{MnO}_3$ film using diffraction methods

H. Himanshu,^{1,2} E. Rebolini,^{1,*} K. Beauvois,³ S. Grenier,⁴ B. Mercey,⁵
B. Domenges †,⁵ B. Ouladdiaf,¹ M. B. Lepetit,^{1,4} and C. Simon²

¹*Institute Laue-Langevin, 71 avenue des Martyrs, 38000 Grenoble, France*

²*Laboratoire National des Champs Magnétiques Intenses (LNCMI-CNRS, Université Grenoble Alpes), 25 avenue des Martyrs, 38000 Grenoble, France*

³*Commissariat à l'Énergie Atomique (CEA), IRIG, MEM, MDN, Univ. Grenoble Alpes, 38000 Grenoble, France*

⁴*Institut Néel (CNRS), 25 avenue des Martyrs, 38000 Grenoble, France*

⁵*CRISMAT, ENSICAEN-CNRS UMR6508, 6 bd. Maréchal Juin, 14050 Caen, France*

(Dated: December 5, 2023)

Supplementary Material

I. CORRECTIONS AND PEAK INTEGRATION METHOD APPLIED TO THE XRD DATA COLLECTED ON LSMO THIN FILM

A. Film area under diffraction

The measured counts/s were normalized with the projection of the beam area onto the sample surface. The general strategy applied is as follows:

- the beam imprint onto the sample (rectangular area) is calculated for both incident and detector sides ;
- the film area that contributes to the measured intensity is the intersection of the smallest area out of the two sides (incident/detector), with the sample surface ;
- These surface areas are calculated using the equations

$$\text{incident beam area} = \frac{h_{slit}}{\cos \chi} \times \frac{v_{slit}}{\sin \omega} \quad (1)$$

$$\text{beam area on the detector} = \frac{h_{slit}}{\cos \chi} \times \frac{det_{vslit}}{\sin 2\theta} \quad (2)$$

where, h_{slit} , v_{slit} and det_{vslit} are respectively the horizontal incident, vertical incident and vertical detector slit sizes (mm), χ is the angle of the out-of-plane sample rotation, ω is the angle of the incident beam with respect to film surface, and 2θ is the angle of the detector with incident beam.

B. Lorentz factor and polarization

To perform these corrections, each data point (counts/s) is divided by

$$\frac{1 + A \cos^2 2\theta}{(1 + A) \sin 2\theta}$$

also known as the Lorentz polarization factor. $A = \cos^2 2\theta_M$ where θ_M is the Bragg angle of the monochromator crystal [? ?]. In our experiment, a Ge (220) monochromator was used for the out-of-plane geometry. Since it was a double bounce monochromator, the final polarization correction includes $A = \cos^4 2\theta_M$ for the out-of-plane reflections.

* rebolini@ill.fr

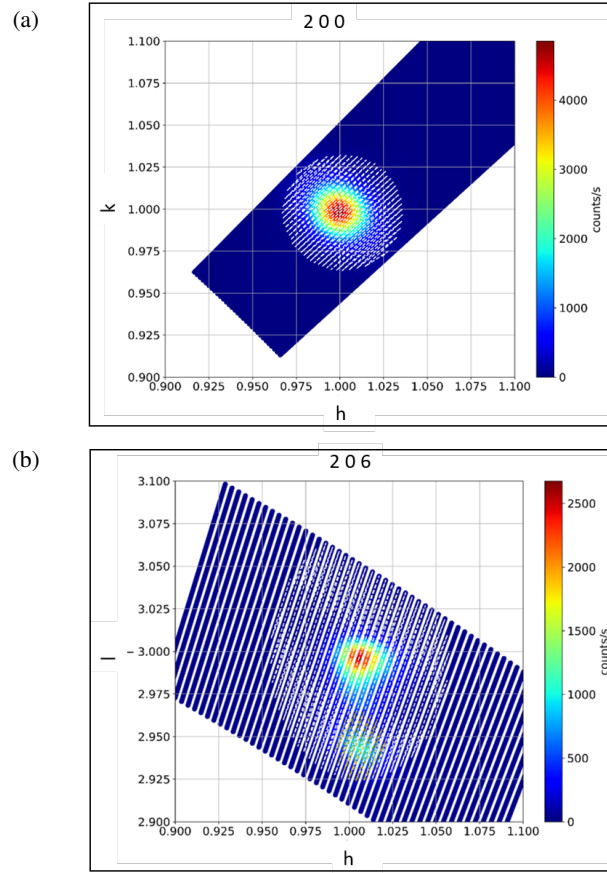


FIG. 1. Two of the measured XRD peaks of the LSMO film with area of integration shown as a dashed circle. (a) (200) peak and (b) (206) peak. The axes are labeled in the STO unit cell because the sample was aligned using the STO unit cell setting.

C. Divergence correction

For the in-plane geometry, the reflections were measured in two separate experiments. In order to make the two data-sets comparable, it has to be made sure that the optical set-up is similar for both. The only difference in the two experiments was the width of slits used for horizontal divergence on the detector side (0.5° and 0.228°). This means that more photons were counted in the measurements with the 0.5° slit. Therefore, all the data points from this set were multiplied with the $0.228/0.5$ factor.

D. Peak integration method

The integration strategy is to first define a radius of integration for each peak. The final intensity is basically the sum of counts/s inside this radius after subtracting the background. The average background is calculated from the data points outside the peak radius (see figure 1).

E. Absorption correction

The integrated intensities were corrected for the x-ray absorption by the film. This was done using the Beer-Lambert's law

$$I = I_0 \exp(-\mu t) \quad (3)$$

Where, I is the measured intensity after absorption, μ is the linear absorption coefficient [?] and t is the thickness of the material under diffraction. For the thin film, the path traveled by X-rays inside the material is $2t/\sin \theta$. Hence, the corrected intensity is given by

$$I_0 = I / \exp(-2\mu t / \sin \theta) \quad (4)$$

II. A FEW OF THE OUT-OF-PLANE PEAKS MEASURED USING XRD ON LSMO FILM

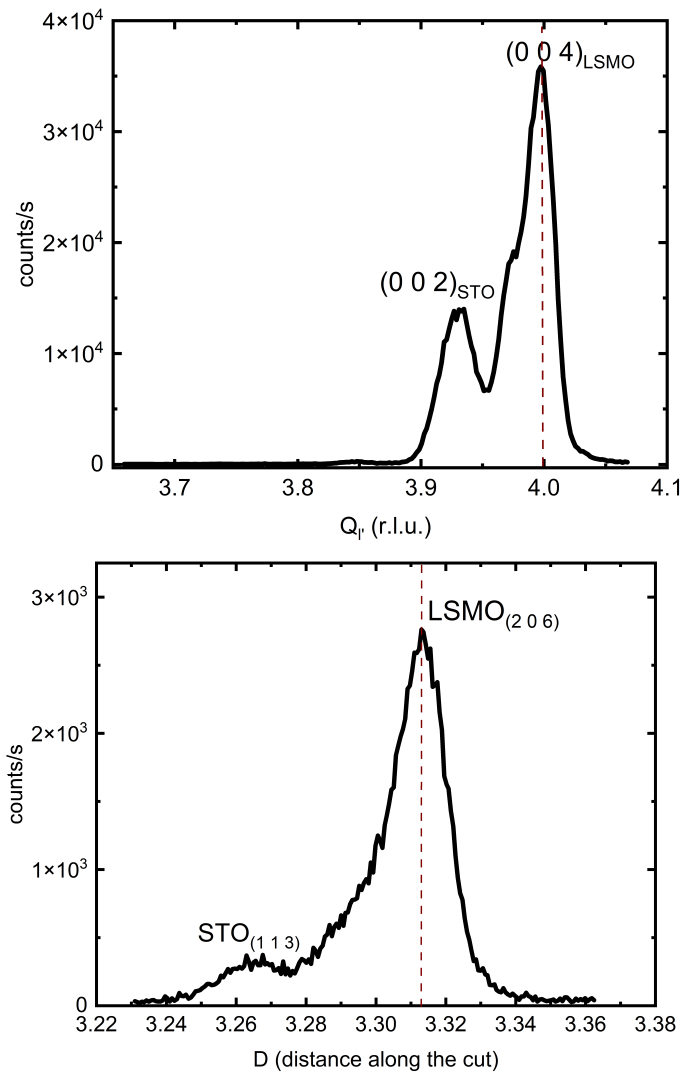


FIG. 2. (a) LSMO (004) XRD peaks and (b) 1D cut of the 2D LSMO (206) scan. One should note the asymmetry seen in out-of-plane LSMO peaks.

III. MAGNETIC HYSTERESIS IN 5 T FIELD

The magnetization curves shown in Figure 3 are for a field applied along [110] and [001] film directions, after subtracting the substrate contribution (i.e. data collected at 300 K). It is clear, from the 'plateau' shape of the magnetization above 2 T, that the moments are saturated in this field.

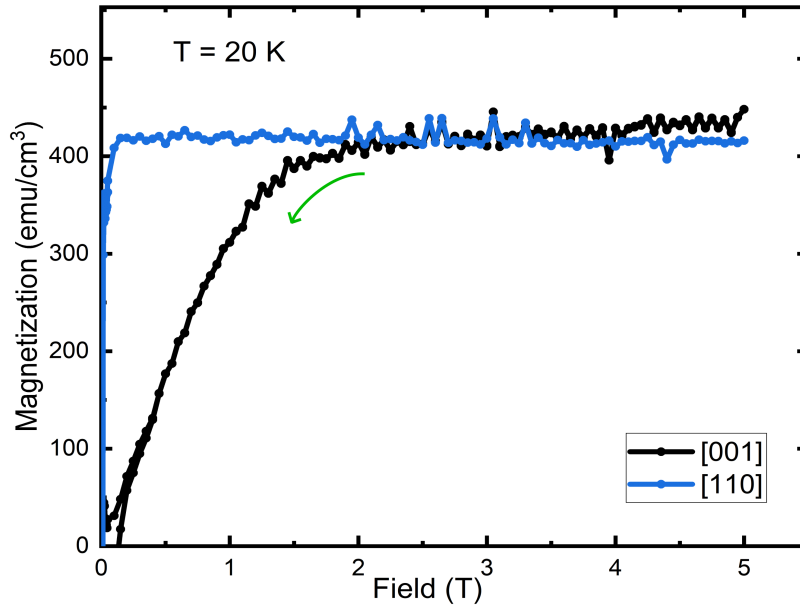


FIG. 3. Magnetization in an applied field up to 5 T, along [110] and [001] directions. Green arrows indicate the direction of the measurement.